Preformation of clusters in heavy nuclei and cluster radioactivity

H. F. Zhang,[1,4,*] J. M. Dong,[1] G. Royer,[2] W. Zuo,[1,3,4] and J. Q. Li[1,3,4]

[1]*School of Nuclear Science and Technology, Lanzhou University, Lanzhou 730000, People's Republic of China*

[2]*Laboratoire Subatech, UMR: IN2P3/CNRS-Université-Ecole des Mines, Nantes 44, France*

[3]*Institute of Modern Physics, Chinese Academy of Science, Lanzhou 730000, People's Republic of China*

[4]*Kavli Institute for Theoretical Physics China, Chinese Academy of Sciences, Beijing 100190, People's Republic of China*

(Received 2 July 2009; revised manuscript received 13 August 2009; published 25 September 2009)

Within the preformed cluster model approach, the values of the preformation factors have been deduced from the experimental cluster decay half-lives assuming that the decay constant of the heavy-ion emission is the product of the assault frequency, the preformation factor and the penetrability. The law according to which the preformation factors follow a simple dependence on the mass of the cluster was confirmed. Then predictions for some of the most possible cluster decays are provided.

DOI: 10.1103/PhysRevC.80.037307 PACS number(s): 23.70.+j, 21.10.Jx, 21.60.Gx, 27.90.+b

Cluster radioactivity (heavy-ion radioactivity) by heavy nuclei with an emitted cluster heavier than an α particle but lighter than fission fragments was first theoretically predicted in the beginning of the 1980s by Sandulescu, Poenaru, and Greiner [1]. The first observation was the detection of ^{14}C emitted from ^{223}Ra by Rose and Jones [2]. Since then, other cluster radioactivities have been observed leading to ^{14}C, ^{20}O, ^{23}F $^{22,24-26}$Ne, ^{28,30}Mg, and ^{32,34}Si emission, and their partial half-lives have been measured. The decaying parent nuclei range from ^{221}Fr to ^{242}Cm at present, all from the translead region, while the daughter nuclei are almost closed shell spherical nuclei. This indicates that shell effects play a key role in selecting possible cluster emissions, and the study of cluster emission can be used to identify shell effects including the very weak subshell closures [3–5]. Several theoretical approaches can be employed to investigate cluster emission: among them the preformed cluster model (PCM) [3,5,6], in which the cluster is assumed to be preformed in the parent nucleus and the preformation factor for all possible clusters is calculated by solving the Schrödinger equation for the dynamical flow of mass and charge; the superasymmetric fission model [7–11], which is based on Gamow's idea of barrier penetration; the unified fission model [12–14] (some authors name it the Coulomb and proximity potential model); and a cluster model with a mean-field cluster potential can also provide a good description of cluster emission [15].

In the present work, the cluster decay constant is the product of the assault frequency, the preformation factor, and the penetrability. The potential barrier which governs the heavy-ion emission has been determined using the generalized liquid drop model (GLDM) with the help of the experimental Q value. The GLDM describes the shape evolution from one body to two separated fragments in a unified way. The preformation factor has been extracted from the experimental cluster decay half-lives and from the theoretical determination of the penetrability and the usual assault frequency. As long as the relation between the preformation factor and the cluster decay is valuable, predictions can be given for the possible cluster decays using the Q value from Audi's recent data [16].

The cluster decay constant is defined as [17]

$$\lambda = P_0 \nu_0 P. \tag{1}$$

Imagining the cluster moving back and forth inside the nucleus with a velocity $v = \sqrt{2E/M}$, it presents itself at the barrier with a frequency $\nu_0 = \frac{1}{2R}\sqrt{2E/M}$. R is the radius of the parent nucleus and E is the energy of the cluster corrected for recoil; M is the average value of mass inertia for the cluster, that will be discussed later. The penetration probability P is calculated within the WKB approximation. The potential barrier governing the cluster emission is determined within the GLDM [10,17].

The barrier penetrability P is calculated within the action integral

$$P = \exp\left\{-\frac{2}{\hbar}\int_{R_{\rm in}}^{R_{\rm out}} \sqrt{2B(r)[E(r) - E(\text{sphere})]}dr\right\}, \tag{2}$$

where $R_{\rm in}$ is the distance between the mass centers of the portions of the initial sphere separated by a plane perpendicular to the deformation axis to assume volume conservation of the future fragments. $R_{\rm out}$ is simply $e^2 Z_d Z_c/Q$. The inertia has been chosen as $B(r) = \mu(1 + 1.3 f(r))$ [11] where

$$f(r) = \begin{cases} \sqrt{\frac{R_{\rm cont} - r}{R_{\rm cont} - R_{\rm in}}}, & r \leqslant R_{\rm cont}, \\ 0, & r \geqslant R_{\rm cont}. \end{cases} \tag{3}$$

$R_{\rm cont} = R_1 + R_2$, R_1 and R_2 are the radii of the daughter nucleus and cluster, respectively. The present inertia can simulate a rapid variation of the friction force effects only at the moment of the neck rupture between the nascent fragments. The preformation factor P_0 of a cluster inside the mother nucleus can be estimated from Eq. (1).

The resulting potential barriers for α decay and cluster ^{32}Si emission of ^{238}Pu are displayed in Figs. 1 and 2, respectively. The maximum of the pure Coulomb barrier lies at the touching point between the nascent fragments. The introduction of the proximity forces lower the barrier of 4.9 MeV for $^{238}\text{Pu} \rightarrow \alpha + {}^{234}\text{U}$ and 24.4 MeV for $^{238}\text{Pu} \rightarrow {}^{32}\text{Si} + {}^{206}\text{Hg}$. Further, the peak is shifted toward a more external position. For cluster

*zhanghongfei@lzu.edu.cn

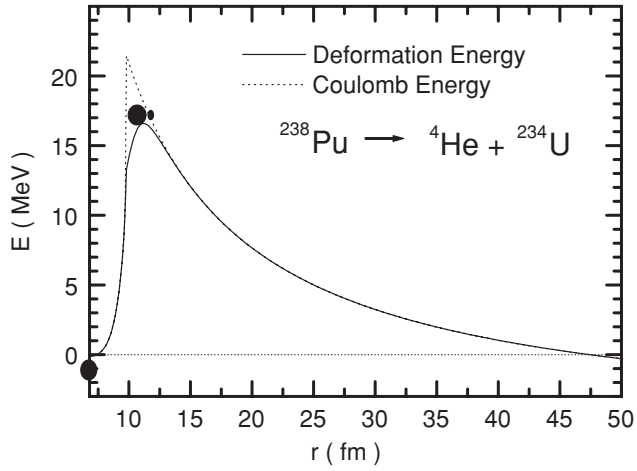

FIG. 1. Potential barrier of α emission from ^{238}Pu with (solid line) and without (dotted line) the proximity energy.

emission, the barrier is lowered by the proximity forces more than that for α decay since the asymmetry is weaker.

In order to estimate the contributions of the proximity forces on the cluster emission as well as on the α decay quantitatively, we calculated the penetrability with and without the proximity energy, respectively. The results are presented in the third column of Table I. The ratio of the penetrabilities with and without the proximity energy ($P^{\mathrm{Def}}/P^{\mathrm{Coul}}$) stands between 2 and 3 for the α decay and increases rapidly with the mass number of the emitted cluster.

The preformation factor may be considered as the overlap of the actual ground state configuration and the configuration representing the cluster coupled to the ground state of the daughter. Obviously it is expected to be much less than unity. The extracted preformation factors from the GLDM are listed in column 5 of Table I, and the results from the DDM3Y model [18] are also listed in the last column for comparison. As can be seen, the preformation factors decrease with the increase of the emitted cluster mass number A_2. Our results are comparable

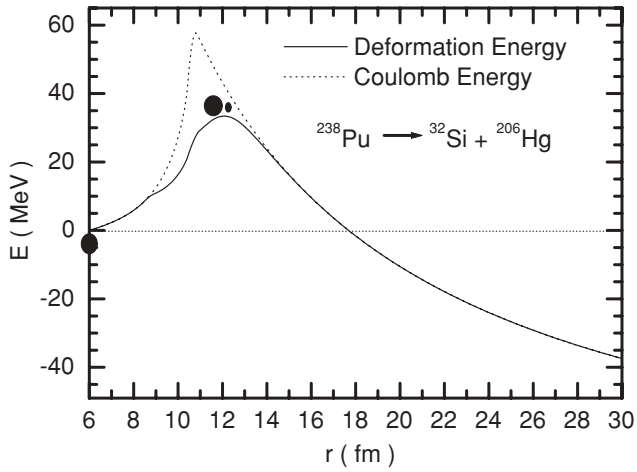

FIG. 2. Potential barrier of ^{32}Si emission from ^{238}Pu with (solid line) and without (dotted line) the proximity energy.

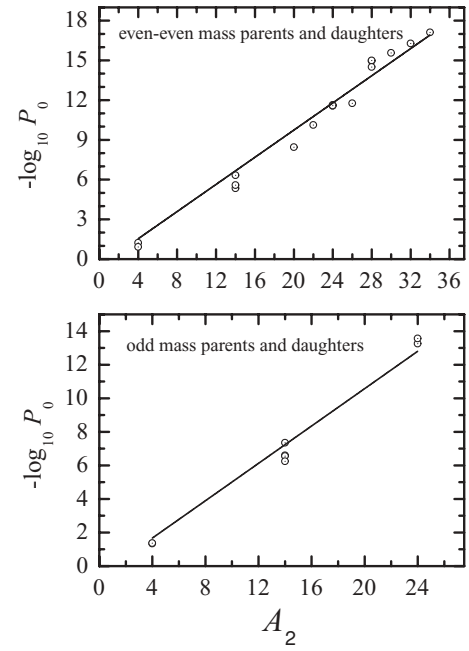

FIG. 3. Negative of logarithm of preformation factors (P_0) as a function of the cluster mass number A_2.

to other values. For example, our calculated value of P_0 for ^{212}Po α emission is 3.405×10^{-2} to be compared with 1.88×10^{-2} [18] and 2.5×10^{-2} deduced in [19]. A value of 3.1×10^{-2} was obtained by Mohr [20] in a double folding model calculation using the density from the experimentally known charge distribution. The general coincidence of the preformation factors from the present results and the DDM3Y calculations is clear.

It has been suggested [21] that, in the case of heavy cluster decay, the preformation factor may scale as

$$P_0 = \left(P_0^{\alpha}\right)^{(A_2-1)/3}, \tag{4}$$

where A_2 is the mass of the cluster and P_0^{α} is the preformation factor for the α decay. Thus a plot of $\log_{10} P_0$ against A_2 should be a straight line. In the upper panel of Fig. 3, the negatives of $\log_{10} P_0$ as well as a best fit line are plotted for decays where both the parent and the daughter are even-even nuclei against the mass number of the cluster. The points fall nearly on a straight line with the P_0^{α} value given by 2.897×10^{-2}. This is comparable to the values 1.93×10^{-2} by Bhattacharya and Gangopadhyay [18] and 1.61×10^{-2} by Poenaru *et al.* [22]. The study has been extended to decays where both the parent and the daughter nuclei have odd mass though the number of observed decays is rather small. The corresponding curve is shown in the lower panel of Fig. 3. Here the S_{α} value is $P_0^{\alpha} = 0.0214$ which is very close to the value $P_0^{\alpha} = 0.0135$ obtained in [18]. With such a linear fit of the logarithm of the spectroscopic factors with mass numbers, we have extended our scheme to calculate the half-lives of some other possible decays where unambiguous lifetime measurements are not yet available and where possibilities of some other decays exist. The results obtained with the GLDM and the fitted values of P_0 from Eq. (4) are tabulated in Table II, compared with the results

TABLE I. Preformation factor P_0 of cluster decay obtained in the present calculation and compared with that of the DDM3Y. The decay energy Q and half-life T are measured in MeV and s, respectively.

Decay	$Q_{\rm expt}$	$P^{\rm Def}/P^{\rm Coul}$	$\log_{10}T_{\rm expt}$	$P_0^{\rm GLDM}$	$P_0^{\rm DDM3Y}$
^{212}Po → ^{4}He + ^{208}Pb	8.950	2.80	−6.52	3.405×10^{-2}	1.88×10^{-2}
^{213}Po → ^{4}He + ^{209}Pb	8.540	2.78	−5.37	2.652×10^{-2}	1.67×10^{-2}
^{214}Po → ^{4}He + ^{210}Pb	7.833	2.45	−3.78	8.734×10^{-2}	3.45×10^{-2}
^{215}At → ^{4}He + ^{211}Bi	8.178	2.50	−4.00	2.467×10^{-2}	1.31×10^{-2}
^{238}Pu → ^{4}He + ^{206}U	5.59	2.14	9.59	1.462×10^{-1}	
^{221}Fr → ^{14}C + ^{207}Tl	31.317	54.71	14.52	2.559×10^{-7}	1.50×10^{-8}
^{221}Ra → ^{14}C + ^{207}Pb	32.396	57.66	13.39	2.808×10^{-7}	1.55×10^{-8}
^{222}Ra → ^{14}C + ^{208}Pb	33.05	64.23	11.00	4.619×10^{-6}	1.64×10^{-7}
^{223}Ra → ^{14}C + ^{209}Pb	31.829	57.50	15.20	4.545×10^{-8}	2.85×10^{-9}
^{224}Ra → ^{14}C + ^{210}Pb	30.54	58.36	15.92	2.614×10^{-6}	1.04×10^{-7}
^{225}Ac → ^{14}C + ^{211}Bi	30.477	35.58	17.34	5.743×10^{-7}	8.14×10^{-8}
^{226}Ra → ^{14}C + ^{212}Pb	28.20	38.21	21.34	4.789×10^{-7}	3.97×10^{-8}
^{228}Th → ^{20}O + ^{208}Pb	44.72	108.54	20.72	3.546×10^{-9}	8.37×10^{-11}
^{230}U→ ^{22}Ne + ^{208}Pb	61.40	166.04	19.57	7.537×10^{-11}	6.72×10^{-12}
^{230}Th → ^{24}Ne + ^{206}Hg	57.571	168.30	24.64	2.310×10^{-12}	1.87×10^{-13}
^{231}Pa → ^{24}Ne + ^{207}Bi	60.417	210.29	23.38	5.542×10^{-14}	3.13×10^{-15}
^{232}U→ ^{24}Ne + ^{208}Pb	62.31	245.73	20.40	2.173×10^{-12}	9.77×10^{-14}
^{233}U → ^{24}Ne + ^{209}Pb	60.486	228.12	24.82	2.725×10^{-14}	1.47×10^{-15}
^{234}U → ^{24}Ne + ^{210}Pb	58.826	215.39	25.25	2.630×10^{-12}	1.54×10^{-13}
^{233}U → ^{25}Ne + ^{208}Pb	60.776	330.45	24.82	3.276×10^{-14}	4.02×10^{-16}
^{234}U → ^{26}Ne + ^{208}Pb	59.466	239.18	25.07	1.755×10^{-12}	1.67×10^{-14}
^{234}U → ^{28}Mg + ^{206}Hg	74.11	296.11	25.74	1.106×10^{-15}	6.30×10^{-17}
^{236}Pu → ^{28}Mg + ^{208}Pb	79.67	464.31	21.67	1.029×10^{-15}	2.83×10^{-17}
^{238}Pu → ^{28}Mg + ^{210}Pb	75.912	395.01	25.70	3.206×10^{-15}	1.21×10^{-16}
^{238}Pu → ^{32}Si + ^{206}Hg	91.19	944.18	25.28	5.343×10^{-17}	2.34×10^{-18}
^{238}Pu → ^{30}Mg + ^{208}Pb	77.00	435.97	25.67	2.733×10^{-16}	2.34×10^{-18}
^{242}Cm → ^{34}Si + ^{208}Pb	96.509	851.74	23.15	7.754×10^{-18}	1.10×10^{-19}

of DDM3Y [18] and the upper limits on experimental half-lives. Except for the case of ^{233}U decay, the results from the two models are all consistent with the experimental observations. In the case of ^{233}U, the results from GLDM and DDM3Y are very coincident, and the discrepancy between theory and experiment is small.

TABLE II. Half-lives of cluster decay obtained with the GLDM and compared with the results of the DDM3Y and experimental data.

Decay	Q (MeV)	$\log_{10}T$ (s) expt.	$\log_{10}T$ (s) GLDM	$\log_{10}T$ (s) DDM3Y
^{223}Ac → ^{14}C + ^{209}Bi	33.065		13.738	
^{223}Ac → ^{15}N + ^{208}Pb	39.474		14.806	
^{224}Th → ^{14}C + ^{210}Po	32.929		14.289	13.68
^{226}Th → ^{14}C + ^{212}Po	30.596		18.461	18.28
^{224}Th → ^{16}O + ^{208}Pb	46.481		15.590	15.47
^{226}Th → ^{18}O + ^{208}Pb	45.727	>16.8	18.381	18.23
^{232}Th → ^{24}Ne + ^{208}Hg	54.497	>29.2	29.654	29.96
^{236}U → ^{24}Ne + ^{212}Pb	55.945	>25.9	29.971	30.16
^{232}Th → ^{26}Ne + ^{206}Hg	55.964	>29.2	28.971	28.57
^{233}U → ^{28}Mg + ^{205}Hg	74.226	>27.6	25.678	26.56
^{237}Np → ^{30}Mg + ^{207}Bi	74.817	>27.6	27.671	27.92
^{240}Pu → ^{34}Si + ^{206}Hg	91.029	>25.5	26.140	26.48
^{241}Am → ^{34}Si + ^{207}Bi	93.926	>24.4	25.778	26.25

New possible islands of cluster emitters around the doubly magic nucleus ^{100}Sn and in the proton and neutron ranges

TABLE III. Predicted half-lives of cluster decay from medium mass nuclei.

Decay	Q (MeV)	$\log_{10}T$ (s)
^{114}Ba → ^{12}C + ^{102}Sn	19.05	11.12
^{114}Ba → ^{16}O + ^{98}Cd	26.50	15.38
^{115}Ba → ^{12}C + ^{103}Sn	18.24	13.55
^{115}Ba → ^{16}O + ^{99}Cd	25.88	17.30
^{116}Ba → ^{12}C + ^{104}Sn	17.22	15.50
^{116}Ba → ^{16}O + ^{100}Cd	24.72	18.88
^{117}Ba → ^{12}C + ^{105}Sn	16.27	18.70
^{117}Ba → ^{16}O + ^{101}Cd	23.54	22.30
^{118}Ba → ^{12}C + ^{106}Sn	15.43	20.85
^{118}Ba → ^{16}O + ^{102}Cd	22.12	25.30
^{119}Ba → ^{12}C + ^{107}Sn	14.34	25.12
^{119}Ce → ^{16}O + ^{103}Sn	27.69	16.17
^{120}Ce → ^{16}O + ^{104}Sn	26.58	17.75
^{121}La → ^{12}C + ^{109}Sb	13.86	28.45
^{121}Ce → ^{16}O + ^{105}Sn	25.49	20.48
^{122}Ce → ^{16}O + ^{106}Sn	24.43	22.29
^{124}Ce → ^{16}O + ^{108}Sn	22.02	28.63
^{125}Pr → ^{16}O + ^{109}Sb	23.09	27.98

$Z = 56$–64 and $N = 58$–72, respectively, have been predicted [23–25]. The first experiment concluded the nonobservation of ^{12}C emission by ^{114}Ba [26]. The predictions for cluster decay half-lives are presented in Table III, which may be useful for future experiments.

To summarize, the heavy ion emission from heavy nuclei has been studied within a preformed cluster approach and the GLDM. The decay constants are obtained from the experimental half-lives. The penetration probabilities are calculated from the WKB approximation and through the potential barriers determined with the GLDM. After using a classical method to estimate the assault frequencies the preformation factors are extracted systematically. Clearly the closed shell structures play a key role for the preformation mechanism. The introduction of the proximity forces lower the barrier of cluster emission far more than that for α decay since the asymmetry is weaker. The law according to which the preformation factors follow a simple dependence on the mass of the clusters was confirmed. Predictions have been made for some possible decays from medium mass nuclei.

This work was supported by the Natural Science Foundation of China (Grants 10775061, 10505016, 10575119, and 10805016), by the Fundamental Research Fund for Physics and Mathematics of Lanzhou University (LZULL200805), the CAS Knowledge Innovation Project No. KJCX-SYW-N02, and the Major State Basic Research Developing Program of China (2007CB815004).

[1] A. Sandulescu, D. N. Poenaru, and W. Greiner, Sov. J. Part. Nucl. **11**, 528 (1980).
[2] H. J. Rose and G. A. Jones, Nature (London) **307**, 245 (1984).
[3] S. Kumar, M. Balasubramaniam, R. K. Gupta, G. Münzenberg, and W. Scheid, J. Phys. G: Nucl. Part. Phys. **29**, 625 (2003).
[4] R. K. Gupta, S. Dhaulta, R. Kumar, M. Balasubramaniam, G. Münzenberg, and W. Scheid, Phys. Rev. C **68**, 034321 (2003).
[5] S. Kumar, R. Rani, and R. Kumar, J. Phys. G: Nucl. Part. Phys. **36**, 015110 (2009).
[6] M. Balasubramaniam and R. K. Gupta, Phys. Rev. C **60**, 064316 (1999).
[7] D. N. Poenaru, M. Ivascu, A. Sandulescu, and W. Greiner, J. Phys. G: Nucl. Part. Phys. **10**, L183 (1984).
[8] W. Greiner, M. Ivascu, D. N. Poenaru, and A. Sandulescu, Z. Phys. A **320**, 347 (1985).
[9] B. Buck and A. C. Merchant, J. Phys. G: Nucl. Part. Phys. **15**, 615 (1989).
[10] G. Royer, R. K. Gupta, and V. Y. Denisov, Nucl. Phys. **A632**, 275 (1998).
[11] G. Royer and R. Moustabchir, Nucl. Phys. **A683**, 182 (2001).
[12] K. P. Santhosh, R. K. Biju, and A. Joseph, J. Phys. G: Nucl. Part. Phys. **35**, 085102 (2008).
[13] K. P. Santhosh and R. K. Biju, J. Phys. G: Nucl. Part. Phys. **36**, 015107 (2009).
[14] J. M. Dong, H. F. Zhang, J. Q. Li, and W. Scheid, Eur. Phys. J. A **41**, 197 (2009).
[15] F. R. Xu and J. C. Pei, Phys. Lett. **B642**, 322 (2006).
[16] G. Audi, A. H. Wapstra, and C. Thibault, Nucl. Phys. **A729**, 337 (2003).
[17] H. F. Zhang and G. Royer, Phys. Rev. C **77**, 054318 (2008).
[18] Madhubrata Bhattacharya and G. Gangopadhyay, Phys. Rev. C **77**, 027603 (2008).
[19] K. Varga, R. G. Lovas, and R. J. Liotta, Phys. Rev. Lett. **69**, 37 (1992).
[20] P. Mohr, Phys. Rev. C **61**, 045802 (2000).
[21] R. Blendowske and H. Walliser, Phys. Rev. Lett. **61**, 1930 (1988).
[22] D. N. Poenaru, Y. Nagame, R. A. Gherghescu, and W. Greiner, Phys. Rev. C **65**, 054308 (2002).
[23] D. N. Poenaru, W. Greiner, and R. A. Gherghescu, Phys. Rev. C **47**, 2030 (1993); D. N. Poenaru, W. Greiner, and E. Hourani, *ibid.* **51**, 594 (1995).
[24] S. Kumar, D. Bir, and R. K. Gupta, Phys. Rev. C **51**, 1762 (1995).
[25] G. Shanmugam, G. M. CarmelVigilaBai, and B. Kamalaharan, Phys. Rev. C **51**, 2616 (1995).
[26] A. Guglielmetti *et al.*, Phys. Rev. C **56**, R2912 (1997).